Efficient solution of three-body quantum collision problems: Application to the Temkin-Poet model

S. Jones and Andris T. Stelbovics

Centre for Atomic, Molecular and Surface Physics, School of Mathematical and Physical Sciences, Murdoch University,
Perth 6150, Australia

We have developed a *variable-spacing* finite-difference algorithm that rapidly propagates the general solution of Schrödinger's equation to large distances (whereupon it can be matched to asymptotic solutions, including the ionization channel, to extract the desired scattering quantities). The present algorithm, when compared to Poet's corresponding *fixed-spacing* algorithm [R. Poet, J. Phys. B **13**, 2995 (1980); S. Jones and A. T. Stelbovics, Phys. Rev. Lett. **84**, 1878 (2000)], reduces storage by 98% and computation time by 99.98%. The method is applied to the Temkin-Poet electron-hydrogen model collision problem. Complete results (elastic, inelastic, and ionization) are obtained for low (17.6 eV), intermediate (27.2, 40.8, and 54.4 eV), and high (150 eV) impact energies.

I. INTRODUCTION

In 1980, Poet [1] introduced a general method for solving the problem of electrons scattering from atoms or ions. In Poet's method, Schrödinger's equation, cast as a set of coupled two-dimensional partial-differential equations in the radial variables of the two electrons, is integrated outward from the atomic center (on a grid with fixed spacing), yielding general, propagating solutions that can be matched to asymptotic solutions to extract the scattering amplitudes. To develop and test his ideas, Poet [1] considered $1s$-$2s$ excitation for model electron-hydrogen collisions that neglect angular momentum [2,3] (now known as the Temkin-Poet model).

In a recent paper [4], we brought Poet's method to completeness for this model problem. Here we generalize Poet's propagation algorithm [1,4] to variable step size, which greatly increases the speed of the algorithm while significantly reducing storage requirements. (Our numerical grid is similar to the one used by Botero and Shertzer [5] in their finite-element analysis of electron-hydrogen scattering.) Although the propagation algorithm, which is independent of asymptotic boundary conditions, can be readily extended to the full electron-hydrogen problem, here we consider the Temkin-Poet model since benchmark calculations for this model problem are needed over a wider range of energies than presented in our previous paper [4]. Results are obtained for low (17.6 eV), intermediate (27.2, 40.8, and 54.4 eV), and high (150 eV) impact energies. These are energies where absolute measurements for electron-hydrogen ionization are available and/or strong theoretical interest exists. (We note that Wang and Callaway [6] extended Poet's fixed-spacing algorithm to the full electron-hydrogen scattering problem; even with this relatively slow fixed-spacing algorithm they were able to obtain very accurate results for the full problem for impact energies below the ionization threshold.)

It is worthwhile here to point out the advantages of the present method as compared to the basic finite-difference method that is presented in most texts on numerical methods. The basic scheme uses a low-order formula, as opposed to

the Numerov formula, to discretize the differential equation (Table I). When applied in two directions to solve our two-dimensional partial-differential equations on a grid with fixed spacing, the Numerov scheme reduces storage by 97% and computation time by 99.9% [7]. In this paper we introduce *variable-spacing* Numerov finite-difference propagation. Using a variable step size in both directions further decreases storage by 98% and computation time by 99.98%.

II. THEORY

We start by writing the Schrödinger equation for the full electron-hydrogen scattering problem (atomic units, with energies in rydbergs, are used in the remainder of this work except where stated otherwise),

$$\left(\nabla_{\mathbf{x}}^2 + \nabla_{\mathbf{y}}^2 + \frac{2}{x} + \frac{2}{y} - \frac{2}{|\mathbf{x}-\mathbf{y}|} + E \right) \Psi(\mathbf{x},\mathbf{y}) = 0. \tag{1}$$

Expanding Ψ as a complete set of functions in $\hat{\mathbf{x}}$ and $\hat{\mathbf{y}}$,

TABLE I. Three-point formulas for discretizing the ordinary second-order differential equation $f''(x) + \phi(x) = 0$, $x \geq 0$, given $f(0) = 0$, and using a step size a. For Coulomb problems, $\phi(0)$ is indeterminate; therefore the usual Numerov formula cannot be used for $x = a$. In this case, the Coulomb singularity should be exhibited explicitly, $f''(x) + 2f(x)/x + \theta(x) = 0$, where $\theta(x) = \phi(x) - 2f(x)/x$ is regular, and the usual Numerov formula ($x > a$) is replaced by the modified one ($x = a$) obtained by constructing a power series for $f(x)$ near the origin [1]. (Basic scheme shown for comparison only; it is not used in this work.)

Scheme	Formula
Basic	$f(x-a) - 2f(x) + f(x+a) + a^2\phi(x) = 0$
Numerov ($x > a$)	$f(x-a) - 2f(x) + f(x+a) + a^2[\phi(x-a)$ $+ 10\phi(x) + \phi(x+a)]/12 = 0$
Numerov ($x = a$)	$(-36 + 54a - 16a^2)f(a) + (18 - 9a - a^2)f(2a)$ $+ a^2[(15 - 8a)\theta(a) + (1.5 - a)\theta(2a)] = 0$

$$\Psi(\mathbf{x},\mathbf{y}) = \frac{1}{xy} \sum_{\ell} \Psi_{\ell}(x,y) Y_{\ell}(\hat{\mathbf{x}},\hat{\mathbf{y}}), \qquad (2)$$

Schrödinger's equation (1) takes the form

$$\left(\frac{\partial^2}{\partial x^2} + \frac{\partial^2}{\partial y^2} \right) \Psi_{\ell}(x,y) + \sum_{\ell'} T_{\ell\ell'}(x,y) \Psi_{\ell'}(x,y) = 0, \qquad (3)$$

where T contains all the nonderivative terms and the index $\ell = 0,1,2,\ldots$ denotes a set of quantum numbers; in particular, $\ell = 0$ corresponds to zero angular momentum for both electrons.

Since $\Psi(\mathbf{x},\mathbf{y})$ must remain finite everywhere, boundary conditions along $x = 0$ and $y = 0$ can immediately be written down for the Ψ_{ℓ},

$$\Psi_{\ell}(x,0) = \Psi_{\ell}(0,y) = 0. \qquad (4)$$

The Pauli exclusion principle demands that Ψ also obey the symmetry condition

$$\Psi(\mathbf{y},\mathbf{x}) = (-1)^S \Psi(\mathbf{x},\mathbf{y}), \qquad (5)$$

depending on whether the two electrons form a singlet (total spin $S = 0$) or triplet ($S = 1$) spin state. Because the wave function is symmetric or antisymmetric under electron exchange, we can solve Schrödinger's equation (3) in just the region $x \geq y$; the symmetry condition (5) then plays the role of a spin-dependent boundary condition along $x = y$. Finally, the asymptotic forms of the $\Psi_{\ell}(x,y)$ for $x \geq y$ are needed to complete the specification of boundary conditions.

In the Temkin-Poet model, the infinite set of coupled equations (3) is reduced to a single equation

$$\left(\frac{\partial^2}{\partial x^2} + \frac{\partial^2}{\partial y^2} + \frac{2}{x} + \frac{2}{y} - \frac{2}{\max(x,y)} + E \right) \Psi_0(x,y) = 0, \quad (6)$$

by keeping only the first term in the expansion (2). For this model problem, the asymptotic boundary condition is easily written down and is given in terms of unknown S-matrix elements by

$$\Psi_0(x,y) \underset{x \to \infty}{\sim} \psi_{\epsilon_m}(y) \phi^*_{k_{\epsilon_m}}(x) - \sum_{n=1}^{\infty} S_{\epsilon_n \epsilon_m} \psi_{\epsilon_n}(y) \phi_{k_{\epsilon_n}}(x)$$

$$- \int_0^E d\epsilon_b S_{\epsilon_b \epsilon_m} \psi_{\epsilon_b}(y) \phi_{k_{\epsilon_b}}(x), \qquad (7)$$

where $\phi_k(x) = (1/\sqrt{k}) \exp(ikx)$ and the ψ_ϵ are bound and continuum states of the hydrogen atom with zero angular momentum,

$$\psi_\epsilon(y) = N_\epsilon [y e^{-qy}\, {}_1F_1(1 - 1/q, 2; 2qy)]. \qquad (8)$$

Here $\epsilon = -q^2$ is the energy of the electron and ${}_1F_1$ is the confluent hypergeometric function. The factor N_ϵ normalizes bound states to unity and continuum states to a δ function in energy,
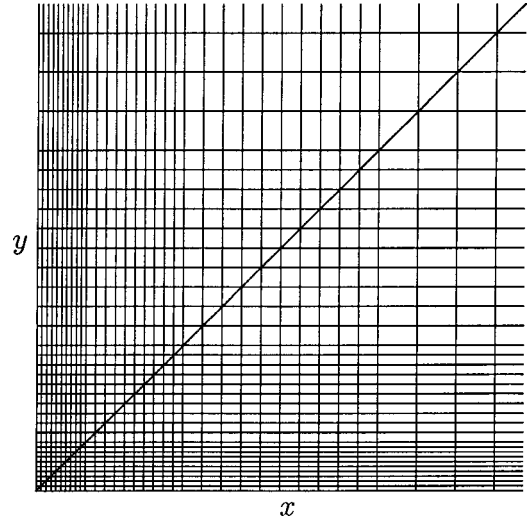

FIG. 1. Schematic diagram of a relatively coarse grid cut off at 10 a.u. in each direction. Here the initial step size $h = 1/10$ a.u. is doubled, at intervals of 10 steps, three times in each direction. For two-electron problems, the computational effort can be reduced by applying a boundary condition imposed by symmetry along the line $x = y$ (shown) and solving the problem in the lower triangular region $x \geq y$.

$$N_\epsilon = \begin{cases} 2/n^3, & -1/n^2 = \epsilon < 0, \\ \sqrt{2/(1 - e^{-2\pi/k})}, & k^2 = \epsilon \geq 0. \end{cases} \qquad (9)$$

Finally, for a given value of ϵ, the momenta k_ϵ in Eq. (7) are fixed by energy conservation according to

$$\epsilon_m + k^2_{\epsilon_m} = \epsilon_n + k^2_{\epsilon_n} = \epsilon_b + k^2_{\epsilon_b} = E. \qquad (10)$$

III. NUMERICAL METHOD

To convert the partial-differential equation (6) into difference equations, we impose a grid with variable spacing (Fig. 1) and approximate derivatives by finite differences. Thus $x \to x_i$ ($i = 0, 1, \ldots$) and $y \to y_j$ ($j = 0, 1, \ldots$), where $x_0 = y_0 = 0$. Since our grid lines are symmetric in x and y, we need only discuss the properties of the grid in a single direction, say x. We define an initial step size h, and consider subsequent doublings of h. Numerous test calculations revealed that (i) the first doubling should be at one atomic unit, (ii) the number of steps before each doubling should be the same, and (iii) the optimal number of doublings is 3. Thus,

$$(\text{step size}) = \begin{cases} h, & 0 \leq x < 1, \\ 2h, & 1 \leq x < 3, \\ 4h, & 3 \leq x < 7, \\ 8h, & 7 \leq x < \infty. \end{cases} \qquad (11)$$

Although the final step size is $8h$, results obtained using this method were just as accurate as those using a grid of fixed spacing h—*the three doublings did not introduce a detectable error*. Thus, in the limit of large propagation distances, the present algorithm is 4096 (8^4) times faster and uses

TABLE II. The nonzero matrix elements of $\mathbf{A}^{(i)}$, $\mathbf{B}^{(i)}$, and $\mathbf{C}^{(i)}$ at grid point (i,j), $j=2,3,\ldots,i$, before applying the boundary condition along $x=y$. The local spacing in the x direction is a and that in the y direction is b. The nonderivative part of the Hamiltonian is $T_j^{(i)}=2/\min(x_i,y_j)+E$. Matrix elements at a junction (a grid line i where the spacing doubles in the x direction) are obtained by replacing $T_{j'}^{(i-1)}$ with $T_{j'}^{(i-2)}$. Matrix elements at a y junction (a grid line j where the spacing doubles in the y direction) are obtained by replacing $j'=j-1$ with $j'=j-2$. To apply the boundary condition along $x=y$, any matrix element in this table corresponding to a grid point lying above the line $x=y$ must be multiplied by $(-1)^S$ and added to the matrix element corresponding to the grid point obtained upon reflection of the out-of-bounds point through $x=y$. At a junction, an additional complication arises for $j=i-2$ and $j=i-1$ in that a point lying above the line $x=y$ reflects to a point on grid line $i-1$ (recall that, at a junction, our formulas can involve only the equally spaced grid lines $i-2$, i, and $i+1$). In this case, Eq. (13) can be used to express the wave function at this point as a linear combination of the wave function at all points on the junction i and $B_{j,j'}^{(i)}\rightarrow B_{j,j'}^{(i)}+(-1)^S A_{j,i-1}^{(i)}D_{i-2,j'}^{(i-1)}$, $(j'=1,2,\ldots,i)$.

j'	$A_{j,j'}^{(i)}$	$B_{j,j'}^{(i)}$	$C_{j,j'}^{(i)}$
$j+1$	$\dfrac{1}{a^2}+\dfrac{1}{b^2}+\dfrac{1}{12}T_{j'}^{(i-1)}$	$\dfrac{10}{b^2}-\dfrac{2}{a^2}+\dfrac{10}{12}T_{j'}^{(i)}$	$\dfrac{1}{a^2}+\dfrac{1}{b^2}+\dfrac{1}{12}T_{j'}^{(i+1)}$
j	$\dfrac{10}{a^2}-\dfrac{2}{b^2}+\dfrac{10}{12}T_{j'}^{(i-1)}$	$-20\left(\dfrac{1}{a^2}+\dfrac{1}{b^2}\right)+\dfrac{100}{12}T_{j'}^{(i)}$	$\dfrac{10}{a^2}-\dfrac{2}{b^2}+\dfrac{10}{12}T_{j'}^{(i+1)}$
$j-1$	$\dfrac{1}{a^2}+\dfrac{1}{b^2}+\dfrac{1}{12}T_{j'}^{(i-1)}$	$\dfrac{10}{b^2}-\dfrac{2}{a^2}+\dfrac{10}{12}T_{j'}^{(i)}$	$\dfrac{1}{a^2}+\dfrac{1}{b^2}+\dfrac{1}{12}T_{j'}^{(i+1)}$

64 (8^2) times less storage to achieve the same accuracy as Poet's fixed-spacing algorithm [1,4].

A. Difference equations

Applying the usual Numerov formula (Table I) to the Schrödinger equation (6) in both the x and y directions, our difference equations at grid line i take the form

$$\mathbf{A}^{(i)}\cdot\mathbf{\Psi}^{(i-1)}+\mathbf{B}^{(i)}\cdot\mathbf{\Psi}^{(i)}+\mathbf{C}^{(i)}\cdot\mathbf{\Psi}^{(i+1)}=\mathbf{0}. \quad (12)$$

Here we have collected the various $\Psi_j^{(i)}$, $j=1,2,\ldots,i$, where $\Psi_j^{(i)}\equiv\Psi_0(x_i,y_j)$, into a vector $\mathbf{\Psi}^{(i)}$. At a junction (a grid line i where the spacing doubles), our difference equations still have the form (12), except that $\mathbf{\Psi}^{(i-2)}$ replaces $\mathbf{\Psi}^{(i-1)}$. This is because our three-point formula (Table I) can involve only equally spaced points if we are to retain the full accuracy of the Numerov scheme. The matrix elements of $\mathbf{A}^{(i)}$, $\mathbf{B}^{(i)}$, and $\mathbf{C}^{(i)}$ for $j>1$ are given in Table II. For $j=1$, but $i\neq 1$, the potential becomes singular in the y direction only, so we use the modified Numerov scheme (Table I)

in the y direction, followed by the usual Numerov formula in the x direction to obtain the results in Table III. Finally, for $i=j=1$, the potential becomes singular in both directions, so we apply the modified Numerov scheme (Table I) in both the x and y directions to obtain the matrix elements of $\mathbf{B}^{(1)}$ and $\mathbf{C}^{(1)}$ given in Table IV [because of the boundary condition along $x=0$, the $\mathbf{A}^{(1)}$ term vanishes in Eq. (12)].

B. Propagating the general solution

By applying symbolic boundary conditions at $x=x_i$, we can solve our equations in terms of $\mathbf{\Psi}^{(i)}$ for $x<x_i$. In particular, we can write

$$\mathbf{\Psi}^{(i-1)}=\mathbf{D}^{(i-1)}\cdot\mathbf{\Psi}^{(i)}, \quad (13)$$

where $\mathbf{D}^{(i-1)}$ is a known (as yet unspecified) matrix. Now using Eq. (13) in Eq. (12), we obtain

$$[\mathbf{B}^{(i)}+\mathbf{A}^{(i)}\cdot\mathbf{D}^{(i-1)}]\cdot\mathbf{\Psi}^{(i)}=-\mathbf{C}^{(i)}\cdot\mathbf{\Psi}^{(i+1)}. \quad (14)$$

TABLE III. The nonzero matrix elements of $\mathbf{A}^{(i)}$, $\mathbf{B}^{(i)}$, and $\mathbf{C}^{(i)}$ for $j=1$ ($i\neq 1$) before applying the boundary condition along $x=y$. The local spacing in the x direction is a and that in the y direction is h ($t\equiv h/a$). Here $\bar{\theta}_j^{(i)}=2/\min(x_i,y_j)+E-2/y_j$. At a junction, replace $\bar{\theta}_{j'}^{(i-1)}$ with $\bar{\theta}_{j'}^{(i-2)}$. For $i=2$, the grid point corresponding to the matrix element $A_{1,2}^{(2)}$ lies above the line $x=y$. This point reflects to the point corresponding to $B_{1,1}^{(2)}$. Thus, $B_{1,1}^{(2)}\rightarrow B_{1,1}^{(2)}+(-1)^S A_{1,2}^{(2)}$.

	$j'=1$	$j'=2$
$A_{1,j'}^{(i)}$	$-36+54h-16h^2+(180-96h)t^2+(15-8h)h^4\bar{\theta}_1^{(i-1)}$	$18-9h-h^2+(18-12h)t^2+(1.5-h)h^4\bar{\theta}_2^{(i-1)}$
$B_{1,j'}^{(i)}$	$-360+540h-160h^2+(-360+192h)t^2+(150-80h)h^4\bar{\theta}_1^{(i)}$	$180-90h-10h^2+(-36+24h)t^2+(15-10h)h^4\bar{\theta}_2^{(i)}$
$C_{1,j'}^{(i)}$	$-36+54h-16h^2+(180-96h)t^2+(15-8h)h^4\bar{\theta}_1^{(i+1)}$	$18-9h-h^2+(18-12h)t^2+(1.5-h)h^4\bar{\theta}_2^{(i+1)}$

TABLE IV. The matrix elements of $\mathbf{B}^{(1)}$ and $\mathbf{C}^{(1)}$ (the case $i = j = 1$) before applying the boundary condition along $x = y$. The local spacing in both directions is h. The grid point corresponding to the matrix element $B_{1,2}^{(1)}$ lies above the line $x = y$. This point reflects to the point corresponding to $C_{1,1}^{(1)}$. Thus, $C_{1,1}^{(1)} \rightarrow C_{1,1}^{(1)} + (-1)^S B_{1,2}^{(1)}$.

$B_{1,2}^{(1)}$	$4(216 - 162h - 21h^2 + 24h^3) + 2(45 - 54h + 16h^2)h^2 \times (E - 1/h)$
$B_{1,1}^{(1)}$	$-16(270 - 549h + 336h^2 - 64h^3) + 4(225 - 240h + 64h^2)h^2(E - 2/h)$
$C_{1,2}^{(1)}$	$4(54 - 63h + 15h^2 + 2h^3) + (9 - 12h + 4h^2)h^2(E - 1/h)$
$C_{1,1}^{(1)}$	$4(216 - 162h - 21h^2 + 24h^3) + 2(45 - 54h + 16h^2)h^2 \times (E - 1/h)$

Comparing Eq. (14) with Eq. (13), we see that the next D matrix, $\mathbf{D}^{(i)}$, is given by

$$\mathbf{D}^{(i)} = -[\mathbf{B}^{(i)} + \mathbf{A}^{(i)} \cdot \mathbf{D}^{(i-1)}]^{-1} \cdot \mathbf{C}^{(i)}. \qquad (15)$$

Thus each $\mathbf{D}^{(i)}$ is generated from the previous one. The first D matrix is given by $\mathbf{D}^{(1)} = -[\mathbf{B}^{(1)}]^{-1} \cdot \mathbf{C}^{(1)}$.

Equation (15) can also be used at a junction if $\mathbf{D}^{(i-1)}$ is replaced with $\mathbf{D}^{(i-2)} \cdot \mathbf{D}^{(i-1)}$ since, using Eq. (13),

$$\mathbf{\Psi}^{(i-2)} = \mathbf{D}^{(i-2)} \cdot \mathbf{\Psi}^{(i-1)} = \mathbf{D}^{(i-2)} \cdot \mathbf{D}^{(i-1)} \cdot \mathbf{\Psi}^{(i)}. \qquad (16)$$

C. Matching to asymptotic solutions

Upon repeated application of Eq. (15), we eventually reach the asymptotic region. In the asymptotic region, Eq. (7) applies and therefore

$$\mathbf{\Psi}^{(i)} \underset{i \to \infty}{\sim} \mathbf{I}^{(i)} - \mathbf{R}^{(i)} \cdot \mathbf{S}. \qquad (17)$$

Here the matrix $\mathbf{I}^{(i)} = \mathbf{R}^{(i)}*$ contains incident waves while $\mathbf{R}^{(i)}$ contains reflected waves,

$$R_{j,n}^{(i)} = \begin{cases} \psi_{\epsilon_n}(y_j)\phi_{k_{\epsilon_n}}(x_i), & n \leq N_d, \\ \int_0^E d\epsilon_b \epsilon_b^p \psi_{\epsilon_b}(y_j)\phi_{k_{\epsilon_b}}(x_i), & n > N_d, \end{cases} \qquad (18)$$

where $p = n - N_d - 1$. Note that the infinite summation over discrete channels is truncated to some finite integer N_d and the quadrature over the two-electron continuum is performed prior to matching by first writing the $S_{\epsilon_b \epsilon_m}$ as a power series in ϵ_b,

$$S_{\epsilon_b \epsilon_m} \approx \sum_{p=0}^{N_c-1} s_{pm} \epsilon_b^p. \qquad (19)$$

The matching procedure, insertion of Eq. (17) into both sides of Eq. (13) and solving for $\mathbf{S}$, then determines the coefficients s_{pm}, rather than $S_{\epsilon_b \epsilon_m}$ directly, which eliminates ill conditioning [1]. In practice, the $i - 1$ equations contained in

the matrix equation (13) far outnumber the $(N_d + N_c)$ unknown scattering coefficients. Following Poet [1], we use all of these equations and solve this overdetermined set for $\mathbf{S}$ by minimizing the sum of the squares of the residuals [the differences between the left- and right-hand sides of Eq. (13) after matching].

IV. RESULTS

Convergence is obtained when the numerical results are no longer sensitive to variations in (i) the initial step size h, (ii) the matching radius x_M, (iii) the number of expansion functions N_c for the continuum, (iv) the number of discrete channels N_d, and (v) the number of energy points N_e in the (Gauss-Legendre) quadrature (18) over the two-electron con-

TABLE V. Singlet $e^- + H(1s) \rightarrow e^- + H(ns)$ cross sections (πa_0^2) for the Temkin-Poet model. Superscripts indicate powers of 10.

	Impact energy (eV)				
n	17.6	27.2	40.8	54.4	150
1	2.245^{-1}	1.313^{-1}	8.648^{-2}	6.472^{-2}	2.011^{-2}
2	3.255^{-2}	1.682^{-2}	8.022^{-3}	4.609^{-3}	6.290^{-4}
3	7.914^{-3}	4.500^{-3}	2.128^{-3}	1.201^{-3}	1.543^{-4}
4	3.022^{-3}	1.830^{-3}	8.665^{-4}	4.864^{-4}	6.135^{-5}
5	1.464^{-3}	9.205^{-4}	4.365^{-4}	2.446^{-4}	3.057^{-5}
6	8.200^{-4}	5.276^{-4}	2.505^{-4}	1.402^{-4}	1.744^{-5}

TABLE VI. Singlet $e^- + H(1s) \rightarrow e^- + e^- + H^+$ SDCS ($\pi a_0^2/\text{Ry}$) for the Temkin-Poet model. Superscripts indicate powers of 10.

	Impact energy (eV)				
ϵ_b/E	17.6	27.2	40.8	54.4	150
0.000	8.142^{-2}	5.574^{-2}	2.656^{-2}	1.481^{-2}	1.819^{-3}
0.025	7.940^{-2}	5.460^{-2}	2.564^{-2}	1.399^{-2}	1.410^{-3}
0.050	7.735^{-2}	5.346^{-2}	2.480^{-2}	1.328^{-2}	1.138^{-3}
0.075	7.524^{-2}	5.231^{-2}	2.402^{-2}	1.264^{-2}	9.485^{-4}
0.100	7.308^{-2}	5.114^{-2}	2.329^{-2}	1.206^{-2}	8.111^{-4}
0.125	7.086^{-2}	4.995^{-2}	2.258^{-2}	1.154^{-2}	7.078^{-4}
0.150	6.858^{-2}	4.875^{-2}	2.191^{-2}	1.106^{-2}	6.278^{-4}
0.175	6.623^{-2}	4.752^{-2}	2.125^{-2}	1.062^{-2}	5.646^{-4}
0.200	6.381^{-2}	4.625^{-2}	2.062^{-2}	1.021^{-2}	5.136^{-4}
0.225	6.132^{-2}	4.495^{-2}	1.999^{-2}	9.832^{-3}	4.719^{-4}
0.250	5.874^{-2}	4.361^{-2}	1.938^{-2}	9.475^{-3}	4.375^{-4}
0.275	5.607^{-2}	4.223^{-2}	1.877^{-2}	9.137^{-3}	4.087^{-4}
0.300	5.332^{-2}	4.080^{-2}	1.817^{-2}	8.812^{-3}	3.843^{-4}
0.325	5.046^{-2}	3.930^{-2}	1.756^{-2}	8.499^{-3}	3.635^{-4}
0.350	4.748^{-2}	3.772^{-2}	1.693^{-2}	8.191^{-3}	3.455^{-4}
0.375	4.434^{-2}	3.602^{-2}	1.629^{-2}	7.866^{-3}	3.297^{-4}
0.400	4.103^{-2}	3.421^{-2}	1.562^{-2}	7.579^{-3}	3.160^{-4}
0.425	3.759^{-2}	3.231^{-2}	1.492^{-2}	7.270^{-3}	3.040^{-4}
0.450	3.426^{-2}	3.041^{-2}	1.420^{-2}	6.963^{-3}	2.940^{-4}
0.475	3.169^{-2}	2.878^{-2}	1.355^{-2}	6.680^{-3}	2.865^{-4}
0.500	3.132^{-2}	2.794^{-2}	1.311^{-2}	6.473^{-3}	2.822^{-4}

TABLE VII. Singlet $e^- + H(1s) \rightarrow e^- + e^- + H^+$ total ionization cross sections (πa_0^2) for the Temkin-Poet model. Superscripts indicate powers of 10.

Impact energy (eV)				
17.6	27.2	40.8	54.4	150
8.418^{-3}	2.140^{-2}	1.946^{-2}	1.472^{-2}	2.926^{-3}

tinuum (by taking $N_e = x_M/a_0$, where $a_0 = 1$ a.u., we obtained four-figure accuracy—using ten times as many points did not change our final results to four significant digits; therefore we consider this particular parameter no further).

For impact energies of 54.4 eV or less, the error in the cross sections due to grid spacing alone is 0.1% or less for $h = 1/20$ a.u. (except for elastic scattering, which required a finer grid and therefore a separate calculation at each energy to obtain this same high precision). To estimate our total uncertainty, we must also take into account the finite matching radius and the finite number of states employed in the matching procedure. For discrete transitions, errors from lack of convergence in x_M, N_c, and N_d are small relative to 0.1%. Thus, for discrete transitions, our total error is still only 0.1%. Turning to ionization, the total error for the singly differential cross section (SDCS) is also 0.1%, except for ϵ_b near $E/2$, where the SDCS is much more sensitive to x_M and N_c than the other observables. As a result, our uncertainty is 1% in the SDCS for $\epsilon_b \approx E/2$ ($0.45 \leq \epsilon_b/E \leq 0.55$). (For an impact energy of 150 eV, we needed a smaller initial step size, $h = 1/40$ a.u., to reduce the error to 0.1%; on the other hand, a considerably shorter matching radius could be used.)

We have performed complete calculations for electrons colliding with hydrogen atoms in the Temkin-Poet model for impact energies ranging from 17.6 to 150 eV. Our precise impact energies are 17.6, 27.212, 40.817, 54.423, and 150 eV (our intermediate total energies are exactly 1, 2, and 3 Ry). Our results, accurate to 0.1% (1% for $\epsilon_b \approx E/2$), are presented in Tables V–X, where superscripts indicate powers of 10. Comparative data for inelastic scattering cross sections have been given by Callaway and Oza [8] and Bray and Stelbovics [9]. Both these references included inelastic cross sections only up to the $n = 3s$ level. Callaway and Oza reported limited results and only for singlet scattering. Bray and Stelbovics presented a compilation of convergent close

TABLE VIII. Triplet $e^- + H(1s) \rightarrow e^- + H(ns)$ cross sections (πa_0^2) for the Temkin-Poet model. Superscripts indicate powers of 10.

n	Impact energy (eV)				
	17.6	27.2	40.8	54.4	150
1	2.112^{+0}	1.159^{+0}	6.315^{-1}	4.039^{-1}	8.125^{-2}
2	4.046^{-3}	5.764^{-3}	5.085^{-3}	4.034^{-3}	1.091^{-3}
3	3.417^{-4}	9.233^{-4}	9.884^{-4}	8.384^{-4}	2.475^{-4}
4	7.941^{-5}	3.075^{-4}	3.592^{-4}	3.132^{-4}	9.567^{-5}
5	2.945^{-5}	1.404^{-4}	1.715^{-4}	1.517^{-4}	4.708^{-5}
6	1.408^{-5}	7.626^{-5}	9.555^{-5}	8.510^{-5}	2.666^{-5}

TABLE IX. Triplet $e^- + H(1s) \rightarrow e^- + e^- + H^+$ SDCS ($\pi a_0^2/Ry$) for the Temkin-Poet model. Superscripts indicate powers of 10.

ϵ_b/E	Impact energy (eV)				
	17.6	27.2	40.8	54.4	150
0.000	9.358^{-4}	7.097^{-3}	9.455^{-3}	8.576^{-3}	2.737^{-3}
0.025	8.107^{-4}	6.173^{-3}	8.064^{-3}	7.121^{-3}	1.845^{-3}
0.050	6.975^{-4}	5.338^{-3}	6.853^{-3}	5.909^{-3}	1.290^{-3}
0.075	5.953^{-4}	4.584^{-3}	5.797^{-3}	4.894^{-3}	9.297^{-4}
0.100	5.035^{-4}	3.908^{-3}	4.877^{-3}	4.041^{-3}	6.847^{-4}
0.125	4.216^{-4}	3.303^{-3}	4.076^{-3}	3.323^{-3}	5.119^{-4}
0.150	3.491^{-4}	2.764^{-3}	3.380^{-3}	2.717^{-3}	3.864^{-4}
0.175	2.853^{-4}	2.287^{-3}	2.776^{-3}	2.205^{-3}	2.931^{-4}
0.200	2.297^{-4}	1.868^{-3}	2.255^{-3}	1.773^{-3}	2.226^{-4}
0.225	1.818^{-4}	1.502^{-3}	1.807^{-3}	1.409^{-3}	1.686^{-4}
0.250	1.409^{-4}	1.186^{-3}	1.424^{-3}	1.103^{-3}	1.270^{-4}
0.275	1.065^{-4}	9.158^{-4}	1.100^{-3}	8.473^{-4}	9.462^{-5}
0.300	7.819^{-5}	6.883^{-4}	8.286^{-4}	6.360^{-4}	6.935^{-5}
0.325	5.532^{-5}	5.000^{-4}	6.044^{-4}	4.631^{-4}	4.960^{-5}
0.350	3.738^{-5}	3.476^{-4}	4.228^{-4}	3.239^{-4}	3.422^{-5}
0.375	2.377^{-5}	2.279^{-4}	2.794^{-4}	2.143^{-4}	2.241^{-5}
0.400	1.387^{-5}	1.371^{-4}	1.698^{-4}	1.306^{-4}	1.359^{-5}
0.425	7.035^{-6}	7.189^{-5}	9.036^{-5}	6.955^{-5}	7.307^{-6}
0.450	2.667^{-6}	2.884^{-5}	3.733^{-5}	2.861^{-5}	3.185^{-6}
0.475	3.934^{-7}	5.426^{-6}	7.871^{-6}	5.850^{-6}	8.604^{-7}
0.500	0.000^{+0}	0.000^{+0}	0.000^{+0}	0.000^{+0}	0.000^{+0}

coupling (CCC) results over a wide range of energies but differing slightly from the energies reported here. Comparing their data with our Tables V and VIII, their calculated cross sections for $1s \rightarrow 1s$, $2s$ are reliable to 2%. The $1s \rightarrow 3s$ singlet cross section of Callaway and Oza is less accurate and at 3 Ry, for example, is in error by about 9% whereas the Bray and Stelbovics $1s \rightarrow 3s$ cross sections are correct to within 3%. It should be emphasized that all the inelastic cross sections up to and including $n = 6$ shown in Table V and Table VIII are accurate to 0.1%.

Singlet and triplet SDCS's are given in Tables VI and IX. The 40.8 eV and 54.4 eV SDCS's were previously reported [4] and compared with the exterior complex scaling (ECS) method [10] and the convergent close coupling calculation of Bray [11]. The ECS calculation is generally in good agreement with our method except at extreme asymmetric energy sharing where the ECS SDCS overshoots by about 10–20%. A new method of amplitude calculation in the ECS method appears to have corrected this discrepancy with our results [12]. The singlet and triplet SDCS's reveal interesting behav-

TABLE X. Triplet $e^- + H(1s) \rightarrow e^- + e^- + H^+$ total ionization cross sections (πa_0^2) for the Temkin-Poet model. Superscripts indicate powers of 10.

Impact energy (eV)				
17.6	27.2	40.8	54.4	150
3.668^{-5}	9.826^{-4}	2.473^{-3}	3.103^{-3}	2.012^{-3}

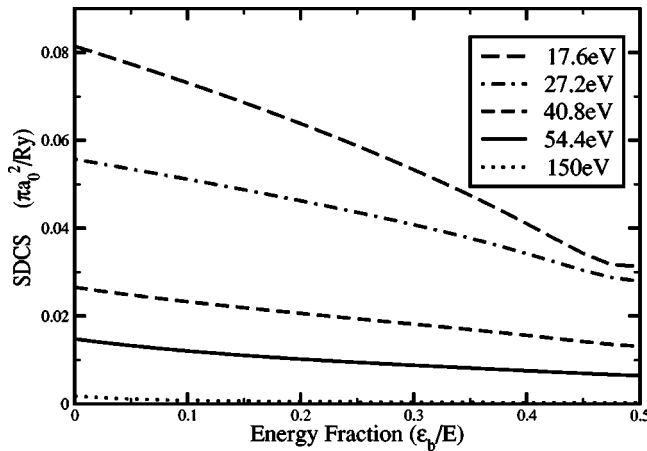FIG. 2. Singlet SDCS ($\pi a_0^2/Ry$) vs energy fraction ϵ_b/E for the impact energies shown.

FIG. 3. Triplet SDCS ($\pi a_0^2/Ry$) vs energy fraction ϵ_b/E for the impact energies shown.

ior as a function of energy which is better demonstrated by their plots in Figs. 2 and 3, respectively. The singlet SDCS as a function of energy changes its shape in a regular way as the energy increases. The 17.6 eV SDCS curve exhibits the largest SDCS as a function of energy fraction and as we move through to 150 eV the SDCS curves decrease monotonically with energy. Subtle differences in shapes of the curves for energy fractions above ≈ 0.4 occur. For triplet scattering on the other hand, the monotonicity with energy is absent. The 17.6 eV triplet SDCS is the smallest over the range of impact energies considered and increases with energy as evidenced by the 27.2 eV and 40.8 eV SDCS plots. By 54.4 eV the SDCS is consistently smaller and the trend continues to 150 eV. From these results it is clear that the triplet ionization cross section is suppressed relative to the singlet ionization cross section at low energies. It is also apparent that there are still significant exchange effects at play at the highest energy of 150 eV.
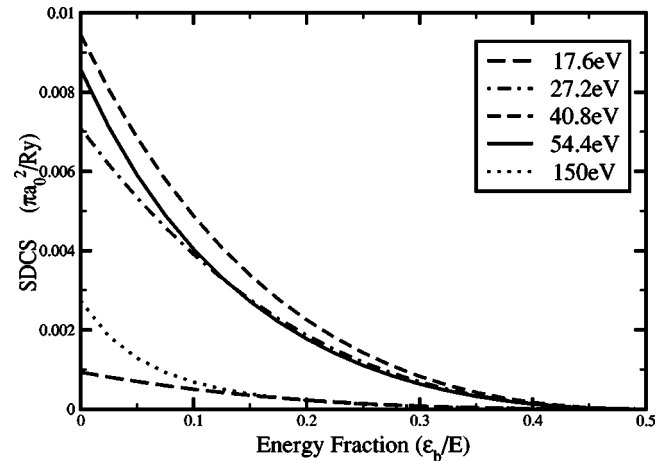
V. SUMMARY

Benchmark calculations have been provided for the Temkin-Poet electron-hydrogen model collision problem over a wide range of collision energies. By integrating Schrödinger's equation on a grid with variable spacing, we increased the speed of Poet's algorithm [1,4] by 3–4 orders of magnitude, while reducing storage requirements by nearly two orders of magnitude. Now that we have optimized our code for this simplified model we can proceed to include angular momentum.

ACKNOWLEDGMENT

[1] R. Poet, J. Phys. B **13**, 2995 (1980).
[2] A. Temkin, Phys. Rev. **126**, 130 (1962).
[3] R. Poet, J. Phys. B **11**, 3081 (1978).
[4] S. Jones and A.T. Stelbovics, Phys. Rev. Lett. **84**, 1878 (2000).
[5] J. Botero and J. Shertzer, Phys. Rev. A **46**, R1155 (1992).
[6] Y.D. Wang and J. Callaway, Phys. Rev. A **50**, 2327 (1994).
[7] S. Jones and A.T. Stelbovics, Aust. J. Phys. **52**, 621 (1999).
[8] J. Callaway and D.H. Oza, Phys. Rev. A **50**, 2327 (1994).
[9] I. Bray and A.T. Stelbovics, At. Data Nucl. Data Tables **58**, 67 (1994).
[10] M. Baertschy, T.N. Rescigno, W.A. Isaacs, and C.W. McCurdy, Phys. Rev. A **60**, R13 (1999).
[11] I. Bray, Phys. Rev. Lett. **78**, 4721 (1997).
[12] C. W. McCurdy, D. A. Horner, and T. N. Rescigno, Phys. Rev. A **63**, 022711 (2001).